On the post-bucking behaviour and imperfection sensitivity of regular convex polygonal columns

R. Gonçalves
CERIS, ICIST and Departamento de Engenharia Civil,
Faculdade de Ciências e Tecnologia, Universidade NOVA de Lisboa, Caparica, Portugal

D. Camotim & André D. Martins
CERIS, ICIST, DECivil, Instituto Superior Técnico
Universidade de Lisboa, Lisboa, Portugal

ABSTRACT: This paper presents and discusses numerical results concerning the elastic post-buckling behaviour and imperfection sensitivity of regular convex polygonal cross-section (RCPS) tubes subjected to uniform compression (columns) and affected by the interaction between local and distortional buckling. As shown previously by the authors, these tubes are characterised by duplicate bifurcation modes (either local or distortional) and, for some geometries, local and distortional buckling may occur simultaneously (local-distortional interaction). A particularly efficient Generalised Beam Theory (GBT) non-linear formulation, specialised for RCPS tubes and employed earlier to characterise their bifurcation behaviour, is used in this work to help pinpoint the occurrence of possible coupling phenomena. The post-buckling results presented and discussed concern columns with different ratios between the critical local and distortional buckling loads, and containing critical-mode initial geometrical imperfections. They are obtained by means of ABAQUS shell finite element analyses and make it possible to draw a set of conclusions on the post-buckling behaviour of RCPS columns affected by local-distortional interaction.

1 INTRODUCTION

Thin-walled tubes with regular convex polygonal cross-sections (RCPS) are widely used in the construction industry, namely in towers and posts supporting lighting equipment and overhead power lines. Although it is undeniable that the local (plate-type) buckling and post-buckling behaviour of hollow-section members (including RCPS members) is nowadays very well understood (e.g. Timoshenko & Gere 1961 or Wittrick & Curzon 1968), with the corresponding knowledge already adequately reflected in the current design specification worldwide, the same is not true as far as the distortional buckling and post-buckling behaviour of RCPS members is concerned.

In order to contribute towards bridging this gap, the authors carried out, in the last few years, an in-depth investigation aimed at characterising the structural behaviour of RCPS tubular members taking advantage of the unique modal decomposition features provided by Generalised Beam Theory (GBT – see, e.g., Schardt 1989, Camotim *et al.* 2010a,b, Gonçalves *et al.* 2010 or Gonçalves & Camotim 2012). Such investigation (Gonçalves & Camotim 2013a,b,c and 2014) unveiled striking and surprising peculiar behavioural features, namely that RCPS members (i) may indeed be susceptible to cross-section distortion (in-plane and out-of-plane deformation), (ii) exhibit duplicate local and distortional buckling (as well as vibration) modes for a wide range of geometries with practical interest, and (iii) are prone to the interaction between local and distortional buckling (nearly coincident local and distortional critical buckling loads). Therefore, their post-buckling behaviour is bound to be affected by local-distortional mode interaction effects and may also exhibit imperfection sensitivity.

This paper presents and discusses the available (preliminary) results of an ongoing numerical investigation on the elastic post-buckling behaviour and imperfection sensitivity of RCPS tubes subjected to uniform compression and affected by local-distortional interaction effects. The work is carried out in the context of the Research Fund for Coal and Steel (RFCS) project RFCS-2015-709892 "Overall-Slenderness Based Direct Design for Strength and Stability of Innovative Hollow Sections – HOLLOSSTAB", which is funded by the European Commission.

The outline of the paper is as follows. Section 2 provides a brief review of the main features exhibited by the bifurcation behaviour of RCPS columns, based on results obtained by means of a computationally efficient geometrically non-linear GBT formulation, specialised for such members. Section 3, devoted to the local and/or distortional post-buckling behaviour of RCPS columns, presents and discusses results obtained from refined ABAQUS (Simulia Inc. 2008) S4 shell finite element analyses and taking into account critical-mode initial geometric imperfections. Finally, Section 4 lists and highlights the most important findings of the work carried out.

2 BIFURCATION BEHAVIOR

Following previous work by the authors (Gonçalves & Camotim 2013a,b,c, 2014), Figure 1 shows the notation employed for the parameters defining the cross-section geometry (*r*, *t*, *b*, *n*) and the GBT discretisation (*m*) for the calculation of local deformation modes. Furthermore, the following non-dimensional geometrical parameters are defined,

$$\beta_1 = \frac{L}{r}, \qquad \beta_2 = \frac{r}{t}, \tag{1}$$

where L is the column (tube) length. In all cases, the material parameters used are $E = 210$ GPa and $\nu = 0.3$.

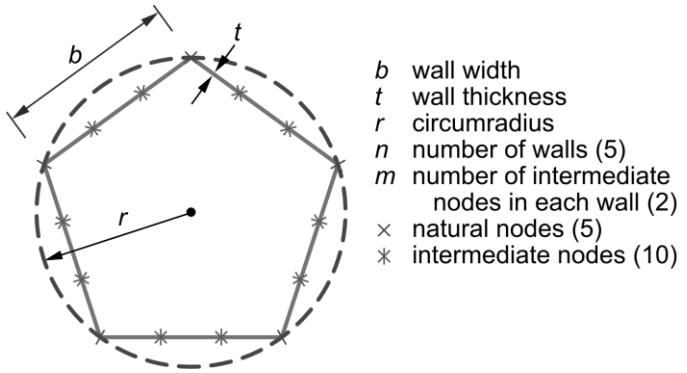

Figure 1. Regular convex polygonal section (RCPS) parameters.

Concerning the RCPS member GBT analysis, Gonçalves & Camotim (2013a) showed that it is possible to use a GBT-based procedure much more efficient than that employed by the conventional GBT. In particular, the cross-section "deformation modes" are obtained very fast and the equilibrium equations become almost fully uncoupled. This stems from the rotational symmetry of the cross-section (of order *n*), leading to symmetric circulant and block-circulant GBT modal stiffness matrices.

Concerning the bifurcation of uniformly compressed RCPS tubes, the focus here is on the standard benchmark problem of simply supported columns, for which sinusoidal modal amplitude functions constitute exact solutions, thus enabling to obtain semi-analytical solutions. This semi-analytical approach enables the acquisition of unique and in-depth information concerning the problem under scrutiny. For instance, the bifurcation stress associated with a buckling mode consisting of a single deformation mode k is given by

$$(\sigma_b)_k = \frac{-1}{X_{kk}}\left(\frac{a^2\pi^2}{L^2}C_{kk} + D_{kk} + \frac{L^2}{a^2\pi^2}B_{kk}\right), \tag{2}$$

where B_{kk}, C_{kk}, D_{kk} and X_{kk} are the GBT stiffness coefficients pertaining to mode k, and a is the buckling mode longitudinal half-wave number. The minimum buckling load and corresponding half-wave length are given by (Schardt 1994)

$$(\sigma_b)_{k,\min} = \frac{D_{kk} + 2\sqrt{C_{kk}B_{kk}}}{X_{kk}}, \quad \frac{L}{a} = \pi\sqrt[4]{C_{kk}/B_{kk}}. \tag{3}$$

For illustrative purposes, Figure 2(a) shows a typical "signature curve" (thick line), providing the variation of the critical bifurcation load with the normalised longitudinal half-wave length, as well as several individual mode solutions (thin lines). The figure also displays representative buckling mode shapes (for simplicity, only half of the columns are represented). These results show that, as the normalised longitudinal half-wave length (β_1/a) increases, the critical buckling modes are either (i) local, (ii) distortional with 6 half-waves around the cross-section, (iii) distortional with 4 half-waves around the cross-section (which becomes "flattened"(or (iv) global (flexural).

Figure 2(b) shows a remarkable (and surprising) result: as in the well-known case of flexural buckling, both local and distortional buckling modes also appear in pairs that share the same stiffness. It can be shown that (i) the critical local buckling mode is always duplicate for odd n and (ii) the critical distortional buckling

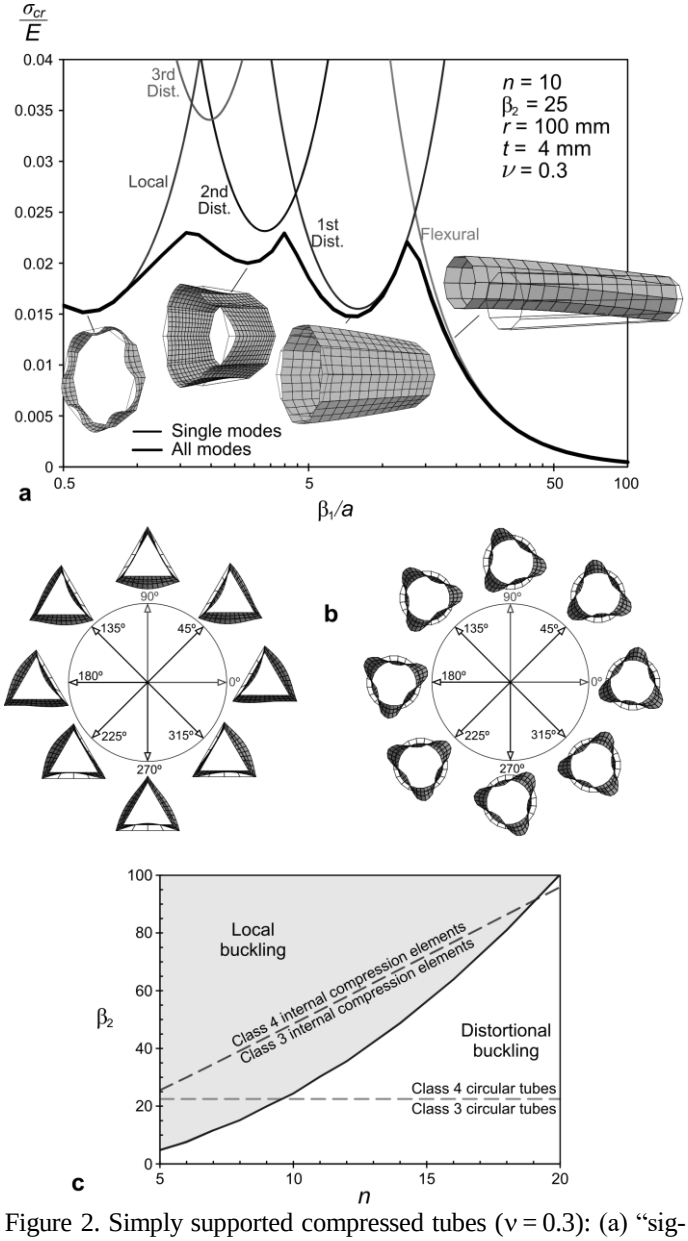

Figure 2. Simply supported compressed tubes ($\nu = 0.3$): (a) "signature" curve, individual mode curves and buckling mode shapes, (b) first local ($n = 3$) and second distortional ($n = 20$) two-dimension buckling mode spaces, and (c) parameter ranges associated with local or distortional critical buckling.

mode is always duplicate for $n > 4$. Naturally, a two-dimension (buckling mode) space is defined by each duplicate solution and any mode lying in such space constitutes a possible critical buckling mode. In particular, Figure 2(b) shows the shapes of some of these modes for the first local ($n = 3$) and second distortional ($n = 20$) mode spaces, which are a function of the "rotation" occurring inside those spaces.

Finally, the graph in Figure 2(c) makes it possible to assess the β_2 and n value ranges associated with either local or distortional critical buckling. This graph was obtained for $\nu = 0.3$ and using Eq. (2) for each mode separately – therefore, no mode interaction is taken into consideration (this approximation yields small errors, as explained in Gonçalves & Camotim 2013b). Note that (i) tubes with low β_2 and high n values buckle in distortional modes and (ii) the β_2 value corresponding to the critical buckling mode nature transition increases exponentially with n.

The dashed lines n Figure 2(c) correspond to the Eurocode 3 limits separating class 3 and 4 (slender) internal compressed walls and circular tubes made of S460 steel grade (the grade yielding the lowest limits). According to the internal compressed wall criterion, a class 4 cross-section exhibiting a critical distortional buckling mode is only possible for $n > 19$ and $\beta_2 > 90$, whereas a much lower β_2 limit is obtained with the circular tube criterion. Because the behaviour of a RCPS member should approach that of a circular tube as n increases, a smooth transition between the two criteria should take place – this is not the case. Indeed, the difference between the two criteria seems to indicate that RCPS columns with moderate-to-high n values may be of class 4 for n and β_2 values below those provided by the internal compressed wall criterion.

3 POST-BUCKLING BEHAVIOUR

3.1 *Local*

The post-buckling behaviour of RCPS columns buckling in local (plate-type) modes is addressed first. These buckling modes involve no column fold-line in-plane displacements and the walls buckle in modes similar to that exhibited by a simply supported plate, even if the critical buckling load is slightly higher for odd n, especially if n is small (Gonçalves & Camotim 2013b). The post-buckling behaviour associated with this type of buckling mode has been extensively studied in the past, for a wide variety of cross-section shapes. Therefore, it seems fair to expect the local post-buckling behaviour of RCPS columns to be qualitatively similar to that exhibited by members with other cross-sections.

The equilibrium paths depicted in Figure 3 concern (i) RCPS columns with the geometries given in Table 1 and containing critical-mode initial geometrical imperfections with various amplitudes and (ii) simply supported plates with one imperfection. For the $n = 5, 7$ columns, the buckling modes are duplicate, as also shown in Figure 3. Using Figure 2, it is concluded that the cross-section geometries defined by these parameters fall well inside the local buckling domain associated with class 4 cross-sections. The lengths L are equal to five times the buckling mode half-wave length. In each column, the bifurcation loads obtained from the shell finite element and GBT analyses never differ by more than 1.3%.

The comparison between the two sets of equilibrium paths displayed in Figure 3, concerning (i) RCPS columns (critical-mode initial geometrical imperfections with various amplitudes – the maximum total/in-plane

Table 1. RCPS column parameters for local buckling

n	β_2	L (mm)
4	50	354
5	60	350
7	81	350

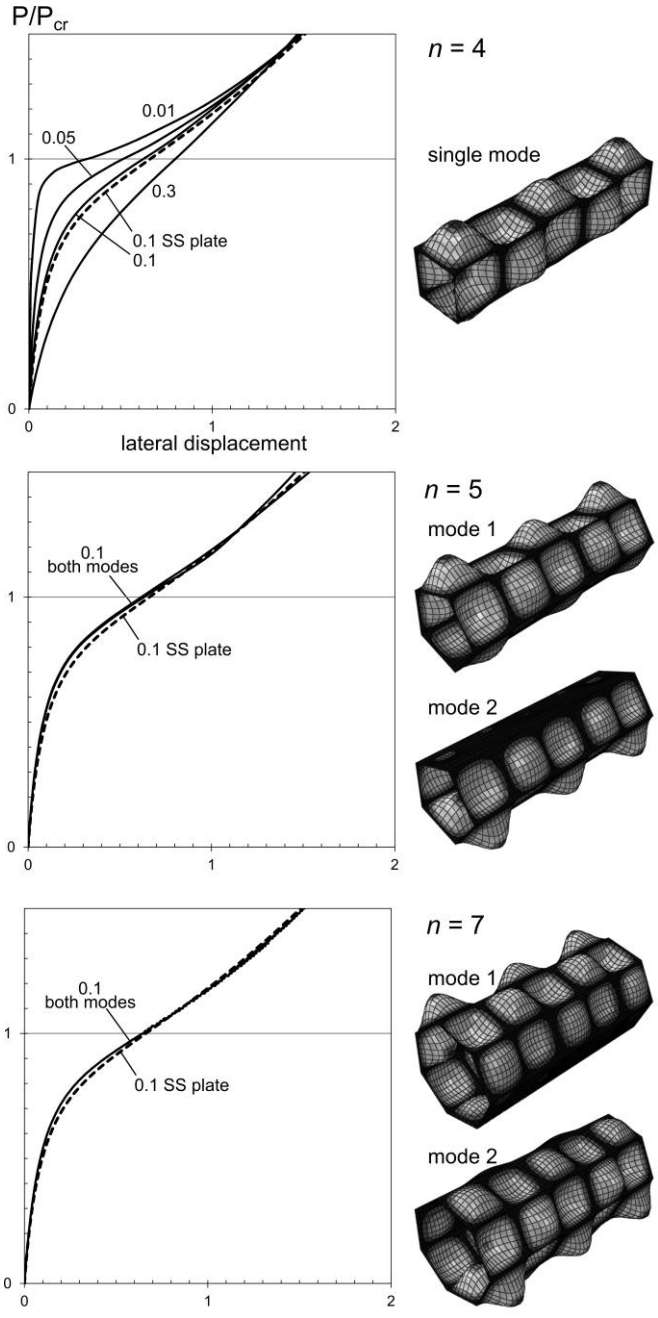

Figure 3. Comparison between the local post-buckling equilibrium paths of RCPS columns with $n = 4, 5, 7$ and simply supported plates with the same length (displacements in mm) (left); and corresponding RCPS column critical buckling mode shapes (right).

displacement) and (ii) simply supported plates (0.1 mm initial imperfections confirms the expected similarity, which can be extended to any other column local post-buckling behaviour. It is also worth noting that the post-buckling behaviour of RCPS columns with odd n values (n = 5, 7), which have duplicate local buckling modes, is not affected by this peculiar behavioural feature. Indeed, the equilibrium paths shown in the second and third plots of Figure 3 are virtually identical to that associated with a "single" buckling mode (n = 4 in this case), irrespective of the imperfection shape adopted (corresponding to duplicate buckling modes).

Therefore, the above elastic local post-buckling equilibrium paths make it possible to conclude that, as expected, RCPS columns are able to sustain applied loads much higher than the critical buckling value. Moreover, it is also logical to expect that the provisions for the design against column local failures currently included in design specifications, namely the effective width and direct strength design approaches, should also provide safe, accurate and reliable local failure load estimates for RCPS columns.

3.2 *Distortional*

The RCPS column distortional post-buckling behaviour is now addressed. Attention is focused on a column geometry characterised by n = 15, t = 2 mm, β_2 = 25 and L = 400 mm, exhibiting a minimum critical distortional bifurcation load associated with duplicate modes (their shapes are displayed in Figure 4). As shown in Figure 2(c), this column geometry falls inside the distortional bifurcation domain and has a class 4 cross-section according to the circular tube criterion. The distortional bifurcation loads calculated by means of the shell finite element and GBT analyses are very close – they differ by only 2.7%.

The equilibrium paths in Figure 4 concern columns containing initial geometrical imperfections with the shapes of each duplicate buckling mode and amplitudes (maximum total displacements, combining in-plane and out-of-plane components) equal to ±0.01 mm – four columns are analysed. At this stage, note that the equilibrium paths monitor a point corresponding approximately to that exhibiting the maximum displacement at the collapse load. It is important to notice that the location of the maximum displacement may change with the applied load level, particularly at the advanced post-buckling stages. The observation of the post-buckling results presented in Figure 4 leads to the following remarks:

(i) The equilibrium path pairs associated with "positive" and "negative" mode 1 and mode 2 initial imperfections are practically coincident and symmetric up to lateral displacements close to 6 mm – Figure 4 shows deformed configurations of the column with "positive" mode 1 imperfections at the equilibrium states A and B (the former concerns the peak load). All equilibrium paths exhibit a slight negative concavity in the close vicinity of the bifurcation load level, which is typically associated with symmetric unstable bifurcations – therefore, it is just logical to expect a mild (critical-mode) imperfection sensitivity of the column failure load.

(ii) Once the 6 mm lateral displacement is reached, the picture changes drastically. Concerning the mode 2 equilibrium paths, the symmetry (with respect to the initial imperfection sign) is suddenly broken: while a very pronounced "snap-back" phenomenon occurs in the "positive" branch, only a moderate slope increase takes place in the "negative" one. The situation is different for the mode 1 equilibrium paths: the symmetry is "more or less" kept, as similar well pronounced "snap-back" phenomena occur in both the "positive" and "negative" branches. However, it is not clear whether the above features are mechanically-based or not, as discussed in the next items.

(iii) It is noted that, regardless of the initial imperfection, the column deformed configuration pattern changes considerably at moderate-to-large displacements, namely once the lateral displacement threshold of approximately 6 mm is reached. In the case of the columns having "positive" imperfections, it was observed that the equilibrium path splits into two branches at state B (see Figure 4) – only the branch that is similar to its "negative" counterpart is shown in the plot. Each branch is associated with deformed configurations displaying two central local buckles

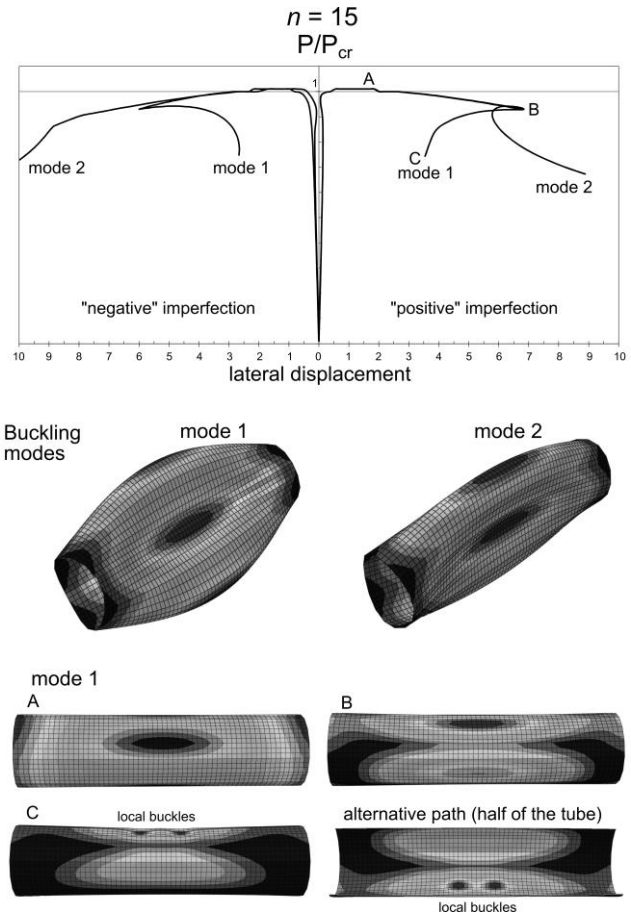

Figure 4. Distortional post-buckling equilibrium paths and critical buckling modes of RCPS columns with n = 15, β_2 = 25 and mode 1 and 2 imperfections (±0.01 mm amplitude); deformed configurations of the column with "positive" mode 1 imperfections.

at one column side – for the column with mode 1 imperfections, they are both depicted at the bottom of Figure 4. The above behavioural features "raise the suspicion" that a secondary bifurcation takes place at equilibrium state B (this should also apply to the "negative" equilibrium paths) – it may happen that the "snap-back" phenomena are just "switches" to (very close) bifurcated paths.

(iv) Another consequence of the column deformed configuration pattern change at moderate-to-large displacements is the fact the particular point monitored (where the displacement is measured) corresponds to various "deformed configuration locations" along the equilibrium paths. It is possible that this location change also causes the "unexpected" features exhibited by the equilibrium paths in Figure 4, namely the abrupt displacement increases/decreases.

(v) To clarify the open questions identified/addressed in the previous items, and also to acquire in-depth insight on the distortional post-buckling mechanics, the authors have under way a GBT-based investigation on this topic – the GBT results modal nature should shed fresh light on this complex problem.

(vi) At this stage, it is worth mentioning that the absence of distortional post-critical strength observed in the RCPS columns contrasts significantly with the well-known moderate-to-high distortional post-buckling strength exhibited by the columns with lipped open cross-sections. Therefore, it may be argued that the post-buckling behaviours of the two column types merely share the designation "distortional", as the underlying mechanics are rather different.

Figure 5 concerns columns with $n = 15$ and $\beta_2 = 25$ containing mode 1 and mode 2 initial imperfections with magnitudes 0.1, 0.2 and 0.5 mm (since the above "unexpected" asymmetries are not mechanically-based, it no longer makes sense to distinguish between "positive" and "negative" initial imperfections) – the purpose is to investigate the influence of the imperfection magnitude. The observation of the results presented in this figure makes it possible to draw the following conclusions:

(i) Despite the much higher imperfection magnitudes, the various equilibrium paths and deformed configurations are qualitatively similar to those depicted in Figure 4 – due to space limitations, no deformed configuration is shown. Moreover, the questions about the mechanics underlying the post-buckling behaviour at moderate-to-large displacements remain open. However, note that the peak load occurs for small/moderate displacements.

(ii) The peak loads associated with the two imperfection shapes virtually coincide. In addition, as expected, the peak load decreases with the imperfection amplitude (and occurs for larger displacements).

(iii) The equilibrium paths associated with mode 2 imperfections exhibit the "unexpected features" mentioned earlier prior to their mode 1 counterparts.

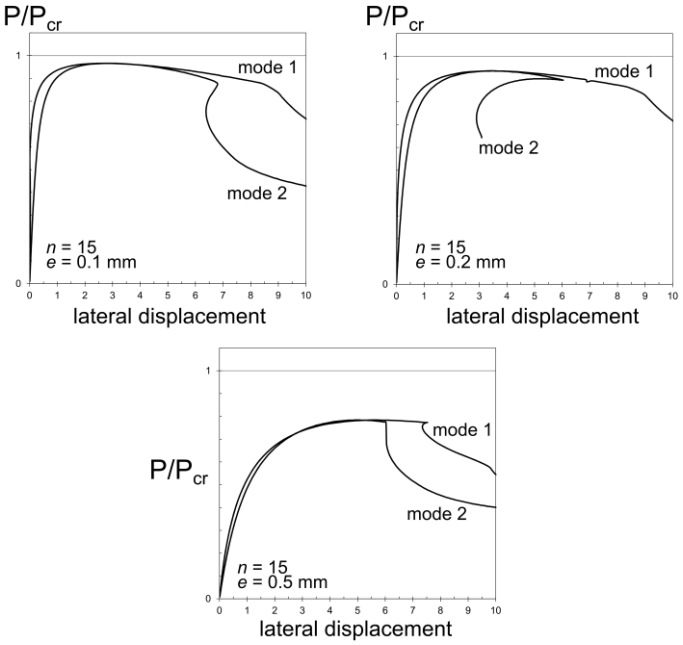

Figure 5. Distortional post-buckling equilibrium paths of RCPS columns with $n = 15$, $\beta_2 = 25$ and containing mode 1 and mode 2 imperfections with several magnitudes.

Consider now RCPS columns with $n = 11$, $t = 2$ mm and $\beta_2 = 25$ – according to Figure 2(c), this column still falls inside the distortional buckling region, although much closer to the local buckling one than the previous column. The duplicate critical buckling loads calculated with the shell model and GBT differ by only 2.2%. As in the previous column, the critical half-wave length is equal to 400 mm (value obtained GBT).

Although this column is "located" fairly close to the local buckling region, note that the local buckling load, calculated by means of GBT, is still significantly higher than the distortional one (20.5%). Moreover, the corresponding half-wave length equals 30 mm, which is not a divisor of 400 mm. However, the local buckling mode of a 400 mm long column exhibits multiple buckles and, thus, the bifurcation is virtually identical to that obtained with a multiple of 30 mm.

The results presented in Figure 6 concern $n = 11$ columns containing several initial imperfections (shapes and magnitudes) and correspond to those displayed earlier, in Figure 4. It is observed that the $n = 11$ column results are very similar to their $n = 15$ column counterparts, namely:

(i) The 0.01 mm equilibrium path exhibits the same small negative curvature.

(ii) The same slight imperfection sensitivity of the column peak load is evidenced.

(iii) At moderate-to-large displacements, the equilibrium path descending branches change significantly and local buckles appear in the column deformed configurations.

It is still worth noting that, in the case of the equilibrium path of the column containing a mode 1 0.01 mm imperfection, the shell finite element analysis unveiled again, for a lateral displacement approximately equal to 6 mm, a split into two branches, each associated with the

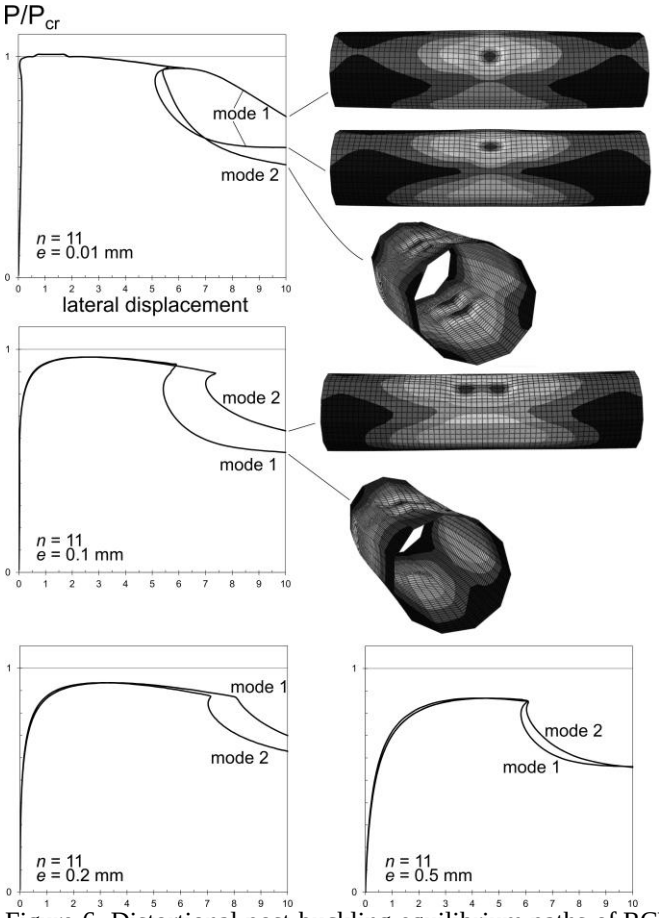

Figure 6. Distortional post-buckling equilibrium paths of RCPS columns with $n = 11$, $\beta_2 = 25$ and containing mode 1 and mode 2 imperfections with several magnitudes.

appearance of a single local buckle at a mid-span cross-section, but with a different location – the corresponding column deformed configurations are depicted in the top right side of Figure 6. As for the column containing a mode 2 0.01 mm imperfection, no branch split was detected and the most deformed configurations exhibit multiple local buckles at diametrically opposite walls – see the third configuration on the right of Figure 6.

The most deformed configuration of the column containing the mode 1 $e = 0.1$ mm imperfection also exhibits local buckles at diametrically opposite walls, whereas its mode 2 counterpart has two closely spaced local buckles appearing in a single wall. The latter deformed configuration is also observed for the two columns containing a 0.2 mm imperfection (mode 1 and mode 2) – they are not shown in Figure 6. Finally, the columns containing 0.5 mm exhibit either one (mode 1) or two (mode 2) local buckles, in both cases appearing in either a single or diametrically opposite walls – these deformed configurations are also not shown in Figure 6. It should be noted that these column deformed configurations resemble that caused by the so-called Brazier effect in circular tubes subjected to bending – of course, in this case the RCPS flattening is due to compression and, thus, local buckles may appear in both sides of the flattened cross-section.

Table 2 shows the normalized peak loads obtained for $n = 11$ and $n = 15$ columns with initial imperfections – because the peak loads are identical for mode 1 and mode 2 imperfections with the same magnitude, only one value is given for each case. The similarity between the P/P_{cr} values of the columns pairs with 0.01, 0.1 and 0.2 mm imperfections is striking. Only the peak loads of the columns with 0.5 mm imperfections differ significantly – the $n = 15$ column P/P_{cr} value is much smaller than its $n = 11$ counterpart (note that the latter column distortional and local critical buckling loads are much closer).

Table 2. Normalised distortional peak loads (P/P_{cr}).

e (mm)	$n = 11$	$n = 15$
0.01	1.010	1.010
0.1	0.965	0.966
0.2	0.935	0.936
0.5	0.867	0.784

3.3 *Local-distortional boundary*

The columns analysed previously exhibit critical (distortional) and second (local) bifurcation loads with differences ranging from 20.5% and 38.1%. This section focuses on columns with much closer distortional and local bifurcation loads, located in the vicinity of the boundary between local and distortional buckling in Figure 2(c).

First, $n = 10$ columns are analysed in detail. For $\beta_2 = 24$ and $L = 350$ mm, the column critical bifurcation load is distortional (duplicate mode) followed by a local one (single mode), which is only 8.7% apart. Thus, it is logical to expect local-distortional interaction effects stronger than before. The results in Figure 7 concern the post-buckling behaviour of columns with the above geometry and containing the same type of initial imperfections considered for the columns analysed earlier. The observation of these results prompts the following comments:

(i) Firstly, the equilibrium paths are much "smoother" than those obtained for the columns analysed previously, in the sense that that the equilibrium path descending branches exhibit no abrupt changes along the whole displacement range.

(ii) For most initial imperfections, the column failure mode (deformed configuration along the descending branch following the peak load) combines a minute cross-section distortion with two local buckles located in diametrically opposite walls – see the first two deformed configurations in Figure 7. However, there are two exceptions, which concern the columns containing 0.5 mm mode 1 or 0.2 mm mode 2 imperfections – their deformed configurations exhibit a single buckle in diametrically opposite walls (see the bottom of Figure 7).

(iii) A slight imperfection sensitivity of the peak load is observed also for this column geometry. The normalised peak loads obtained for the various initial imperfections are given in Table 3. Since the peak loads associated with the two imperfection shapes are again virtually identical, only one value is given for each amplitude.

(iv) The comparison between the normalised peak loads given in Tables 2 and 3 shows that the imperfection sensitivity is marginally higher for the $n = 10$ column

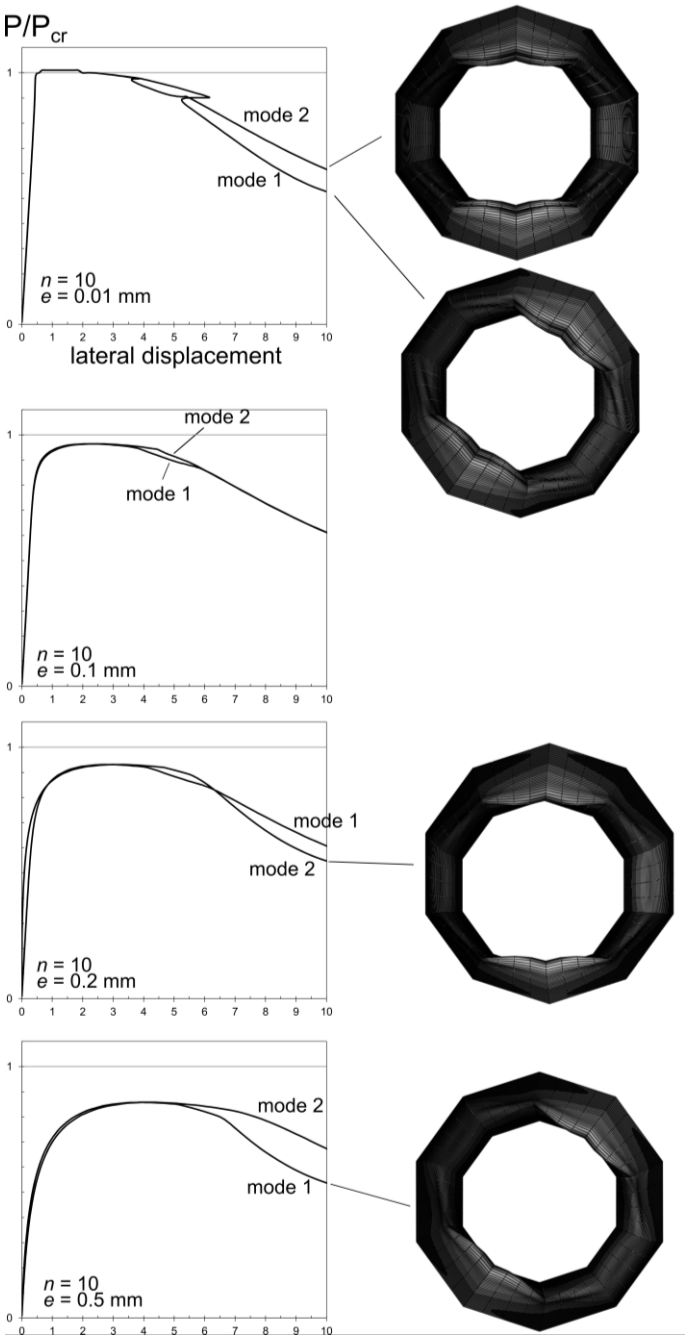

Figure 7. Post-buckling equilibrium paths of RCPS columns with $n = 10$, $\beta_2 = 24$ and containing mode 1 or mode 2 imperfections with several magnitudes.

(slightly lower P/P_{cr} values). However, this does not remain true for the largest imperfection amplitude (0.5 mm): the $n = 10$ column P/P_{cr} value falls (in-between its $n = 11$ and $n = 15$ column counterparts – recall that the latter was unexpectedly low.

(v) After comparing the post-buckling behaviours of the $n = 10$, $n = 11$ and $n = 15$ columns, it is concluded that they are qualitatively and quantitatively quite similar. Indeed, the most noticeable difference lies in the "smoothness" of the $n = 10$ column equilibrium paths (no significant descending branch changes at moderate-to-large displacements). Thus, it seems fair to argue that the post-buckling behaviour of the $n = 10$ column is not meaningfully affected by local-distortional interaction effects – it retains all the distinctive distortional features.

Table 3. Normalized peak loads P/P_{cr} ($\beta_2 = 24$ and $L = 350$ mm).

e (mm)	$n = 10$
0.01	1.010
0.1	0.964
0.2	0.931
0.5	0.858

Finally, a column located "on the local side" of the local-distortional boundary (critical local bifurcation load) is analysed. The particular geometry considered corresponds to $n = 10$, $\beta_2 = 27$ and $L = 400$ mm, and is associated with a critical local bifurcation load (single mode) that is 3.4% above its distortional (duplicate mode) counterpart. In spite of this small bifurcation load difference, note that the first 8 bifurcation loads are local, which means that the duplicate distortional modes correspond to the 9th and 10th bifurcation loads – the shapes of these 10 buckling modes are in the top of Figure 8.

The equilibrium paths shown in the bottom of Figure 8 concern columns having (critical-mode) local initial

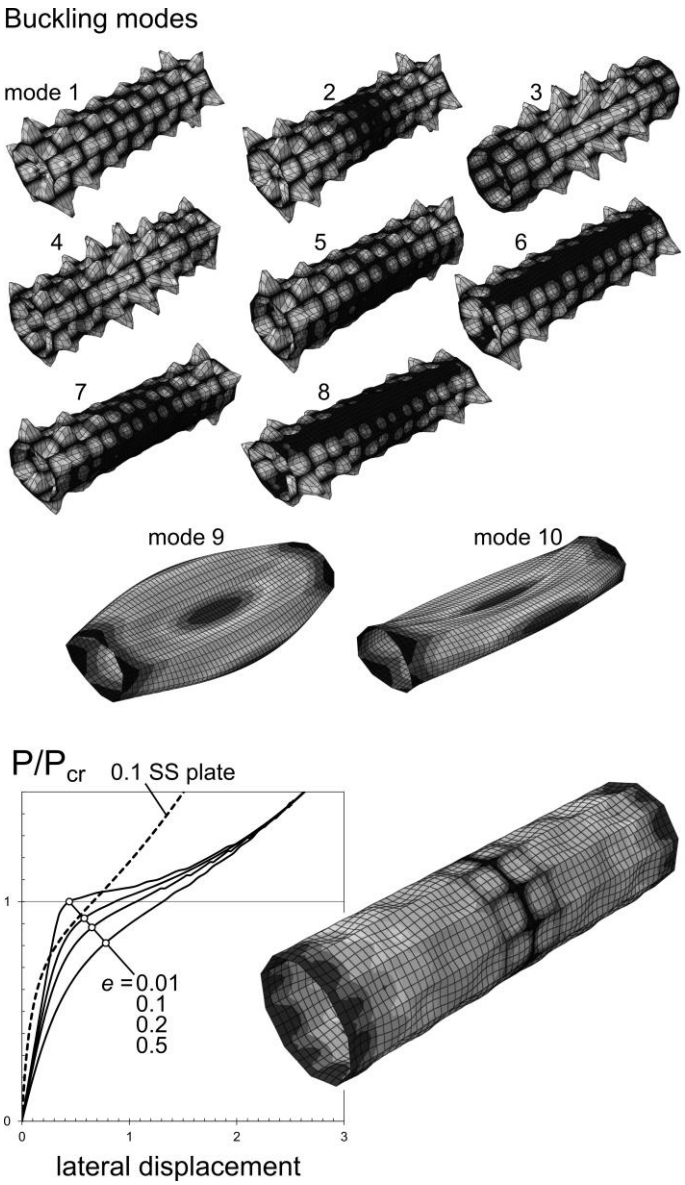

Figure 8. RCPS columns with $n = 10$ and $\beta_2 = 27$: first 10 buckling modes, equilibrium paths of columns with several critical-mode imperfection magnitudes and deformed configuration at $P/P_{cr} = 1.5$.

imperfections with the same amplitudes considered previously: 0.01, 0.1, 0.2 and 0.5 mm. For comparison purposes, the equilibrium path of a simply supported plate with a 0.1 mm initial imperfection is also shown (dashed curve) – note that this equilibrium path had already been shown in Figure 3. Figure 8 also includes a column deformed configuration corresponding to the highest applied load level ($P/P_{cr} = 1.5$) and is shared by the columns with all the imperfection magnitudes – note that all equilibrium paths have merged together at $P/P_{cr} = 1.5$. It can be readily observed that:

(i) Stable equilibrium paths are now obtained, which means that this column is not imperfection sensitive. Nevertheless, it should be noticed that these equilibrium paths are clearly "less stable" than their simply supported plate counterpart, which seems to indicate the presence of strength erosion stemming from local-distortional interaction effects.

(ii) Although no distortional deformations are can be readily detected (even if the applied load level exceeds by far the distortional bifurcation load), their presence is felt through the reduced strength exhibited by the column (with respect to columns with a "pure" local post-buckling behaviour). The authors believe that a GBT-based analysis will unveil the presence of minute distortional deformations in the column deformed configuration. Moreover, it will be also worth obtaining post-buckling results of columns containing distortional initial imperfections.

4 CONCLUSION

This paper presented and discussed the available (preliminary) shell finite element results concerning an ongoing numerical investigation on the elastic local, distortional and interactive (local-distortional) post-buckling behaviour of thin-walled columns with regular convex polygonal cross-sections (RCPS) – the imperfection sensitivity of the column peak load was also addressed. Out of the various findings reported in this work, the following ones deserve to be highlighted:

(i) Depending on the β_2 and n values, either local or distortional buckling may be critical – see Figure 2(c). Columns with low β_2 and high n buckle in distortional modes – the β_2 value associated with mode nature transition increases exponentially with n.

(ii) The column pure local post-buckling behaviour is highly stable and virtually identical to that exhibited by simply supported plates.

(iii) The column pure distortional post-buckling behaviour is slightly unstable and, thus, a small imperfection sensitivity is exhibited by the peak load – this distortional is very different from that of lipped open-section columns. Local deformations are visible after the peak load is reached.

(iv) The post-buckling behaviour of columns with close local and distortional bifurcation loads is either (iv_1) quite similar to the pure distortional one (i.e., minute local-distortional interaction occurs – however, the post peak paths are smoother), for distortional critical buckling, or (iv_2) visibly affected by local-distortional interaction (sizeable post-critical strength/stiffness erosion), for local critical buckling – even if no distortional deformations were spotted.

Further work is currently under way to assess the various RCPS column post-buckling behaviours by means of geometrically non-linear GBT-based post-buckling analyses, which will enable acquiring much more in-depth knowledge about the underlying mechanics, namely those associated with secondary bifurcations and local-distortional interaction.

ACKNOWLEDGMENTS

The financial support of the European Commission, through the Research Fund for Coal and Steel project RFCS-2015-709892, "Overall-Slenderness Based Direct Design for Strength and Stability of Innovative Hollow Sections – HOLLOSSTAB", is gratefully acknowledged.

REFERENCES

Camotim D., Basaglia C., Bebiano R., Gonçalves R. & Silvestre N. 2010a. Latest developments in the GBT analysis of thin-walled steel structures. In E. Batista, P. Vellasco, L. Lima (eds.), *Proceedings of International Colloquium on Stability and Ductility of Steel Structures (SDSS'Rio 2010 – Rio de Janeiro, 8-10/9*): 33-58 (Vol. 1).

Camotim D., Basaglia C., Silva N. & Silvestre N. 2010b. Numerical analysis of thin-walled structures using Generalised Beam Theory (GBT): recent and future developments. In B. Topping *et al.* (eds.), *Computational Technology Reviews*: 315-354 (Vol. 1), Stirlingshire: Saxe-Coburg.

Gonçalves R., Ritto-Corrêa M. & Camotim D. 2010. A new approach to the calculation of cross-section deformation modes in the framework of Generalized Beam Theory, *Computational Mechanics* 46(5): 759-781.

Gonçalves R. & Camotim D. 2012. Geometrically non-linear Generalised Beam Theory for elastoplastic thin-walled metal members, *Thin-Walled Structures* 51: 121-129.

Gonçalves R. & Camotim D. 2013a. On the behaviour of thin-walled steel regular polygonal tubular members, *Thin-Walled Structures* 62: 191-205.

Gonçalves R. & Camotim D. 2013b. Elastic buckling of uniformly compressed thin-walled regular polygonal tubes, *Thin-Walled Structures* 71: 35-45.

Gonçalves R. & Camotim D. 2013c. Buckling behaviour of thin-walled regular polygonal tubes subjected to bending or torsion, *Thin-Walled Structures* 73: 185-197.

Gonçalves R. & Camotim D. 2014. The vibration behaviour of thin-walled regular polygonal tubes. *Thin-Walled Structures* 84: 177-188.

Schardt R. 1989. *Verallgemeinerte Technische Biegetheorie*. Berlin: Springer-Verlag.

Schardt R. 1994. Generalized Beam Theory – an adequate method for coupled stability problems. *Thin-Walled Structures* 19: 161-180.

Simulia Inc. 2008. *ABAQUS Standard* (version 6.7-5).

Timoshenko S. & Gere J. 1961. *Theory of Elastic Stability*. New York: McGraw-Hill.

Wittrick W. & Curzon P. 1968. Local buckling of long polygonal tubes in combined compression and torsion. *International Journal of Mechanical Sciences* 10: 849-857.